Bed-Based Ballistocardiography System Using Flexible RFID Sensors for Noninvasive Single- and Dual-Subject Vital Signs Monitoring

Pablo Escobedo, Antonio Pousibet-Garrido, Nuria López-Ruiz, Miguel A. Carvajal, Alberto J. Palma, and Antonio Martínez-Olmos

***Abstract*— This work presents an innovative approach employing passive radio frequency identification (RFID) technology to develop a comprehensive ballistocardiography (BCG) system for contactless and noninvasive vital sign monitoring of individuals on a mattress. The method relies on wireless energy transfer through inductive coupling at 13.56 MHz between an active powering board and a passive, flexible sensing board with dimensions of 12.6 × 4.7 cm^2. Both boards face each other at a separation distance of 3 cm. The system demonstrates remarkable sensitivity to mattress vibrations resulting from bodily movements, rendering it proficient in generating complete BCG signals capable of discerning heart rate (HR), breathing rate (BR), and activity. Practical trials with six healthy subjects validated the feasibility and efficacy of the system, showing an average absolute error of 1.8 beats/min for HR and 0.6 breaths/min for BR. Unlike conventional BCG systems, the sensing module seamlessly integrates into the mattress side. This is leveraged to enable the simultaneous monitoring of two subjects on a queen-size mattress, taking advantage of the local sensitivity of the sensing mechanism. Extracted BCG values can be wirelessly transmitted to the user's smartphone through near-field communication (NFC) and to a cloud service used for storage, distribution, and categorization of subject data. This work establishes a foundation for future extensive studies and applications, as the obtained BCG signals could provide health-related insights, such as detecting heart diseases, respiratory problems, or evaluating sleep quality.**

***Index Terms*— Ballistocardiography (BCG), energy harvesting, flexible electronics, near-field communication (NFC), noninvasive monitoring, passive system, printed electronics, radio frequency identification (RFID).**

Manuscript received 5 December 2023; revised 19 December 2023; accepted 24 December 2023. Date of publication 23 February 2024; date of current version 14 March 2024. This research was carried out thanks to Project PID2022-138727OB-I00 funded by MCIN/AEI/10.13039/501100011033 and by ERDF "A way of making Europe", grant IJC2020-043307-I, and Junta de Andalucía (Spain) under project PYC20-RE-040UGR. The Associate Editor coordinating the review process was Dr. Nuria Novas. *(Corresponding author: Antonio Martínez-Olmos.)*

This work involved human subjects or animals in its research. Approval of all ethical and experimental procedures and protocols was granted by the Ethics Committee in Human Research (CEIH) of the University of Granada under Application No. 2446/CEIH/2021, and performed in line with the Declaration of Helsinki.

The authors are with the Electronic and Chemical Sensing Solutions Group (ECsens), CITIC-UGR, Unit of Excellence in Chemistry Applied to Biomedicine and the Environment of the University of Granada, Department of Electronics and Computer Technology, University of Granada, 18071 Granada, Spain (e-mail: amartinez@ugr.es).

Digital Object Identifier 10.1109/TIM.2024.3369134

I. Introduction

BALLISTOCARDIOGRAPHY (BCG) is a noninvasive technique used to generate a graphical representation of bodily movements resulting from the propagation of blood within the vasculature during each cardiac cycle. Initial efforts to capture these bodily dynamics were first documented by Gordon [11], followed by Henderson [2]. Nevertheless, the technique did not undergo significant development until 1939 when Starr et al. [3] achieved a breakthrough by recording the longitudinal displacements experienced by a rigid table upon which subjects lay as a consequence of the cardiac impulses, employing a lamp and a camera. The analysis of these recorded ballistic curves, subsequently termed "ballistocardiograms," demonstrated their utility in identifying individuals with abnormal circulatory patterns or cardiac conditions [4]. A comprehensive review of these pioneering experiences can be found in the existing literature [5]. Starr's description ushered in over three decades of substantial investigation into BCG as a cardiac diagnostic tool. However, the advent of newer clinical methods, such as echocardiography, ultrasound, and computerized tomography, offering more precise results, led to the waning interest in BCG [6]. In recent years, the evolution of novel sensors and computational techniques has reignited interest in BCG, expanding its applications beyond clinical contexts [7], [8], to encompass diverse fields, including the automotive and aeronautics industry [9], [10], physiological monitoring of patients with physical constraints [11], e-health [12], assessment of mental fatigue [13], Internet of Things (IoT) [14], operation in microgravity environments [15], and smart homes [16], [17].

One of the primary objectives in the application of BCG has been the detection of heart and breath rates (HR and BR) [18], [19]. BR and HR of subjects lying on a bed can provide valuable insights into an individual's health and well-being. Sudden changes or irregularities in these vital signs can be indicative of various medical conditions, including cardiac issues, respiratory problems, or sleep disorders, such as sleep apnea. On the other hand, activity monitoring can be particularly useful to assess the overall quality of sleep, especially when it comes to understanding sleep patterns and sleep stages [20].

Consequently, substantial efforts have been invested in the development of BCG systems tailored for sleep and vital

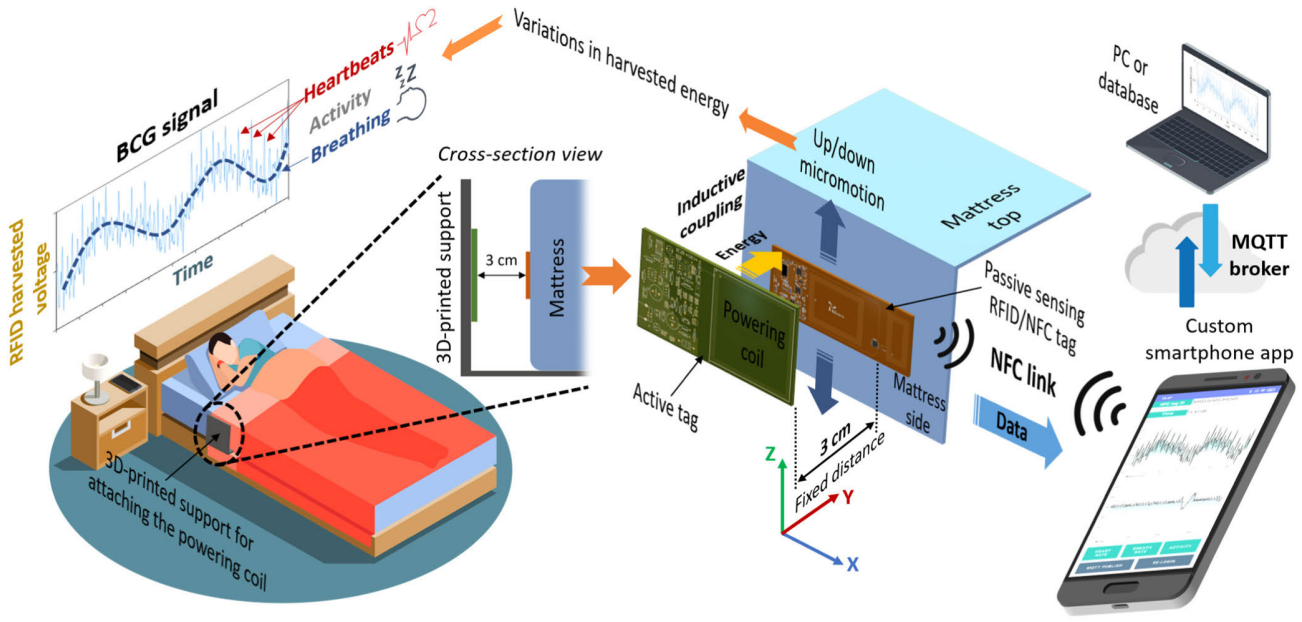

Fig. 1. Overview of the proposed RFID-based BCG system for noninvasive monitoring of a subject's vital signs lying on a bed.

signs monitoring [21], [22]. In these previous systems, a variety of conventional sensors has been employed to generate BCG signals, including electromechanical films (EMFi), strain gauges [23], piezoelectric polyvinylidene fluoride (PYDF) film-based sensors [24], fiber-optic sensors [25], pneumatic and hydraulic-based sensors [26], and optical sensors [27], [28], among others [29]. In light of recent advancements in wireless technologies, alternative methods for monitoring vital signs have emerged, including systems that leverage Wi-Fi signals [30], radar-based sensors [31], and even vision-based approaches [32]. The radio frequency identification (RFID) technology offers distinct advantages, characterized by its lightweight, cost-effectiveness, possibility of battery-less operation, and compact tag design, making it well-suited for unobtrusive sleep monitoring [33].

The main goal of this work is to introduce an innovative approach employing passive RFID technology to establish a comprehensive BCG system designed for contactless and noninvasive monitoring of vital signs in individuals lying on a mattress. The developed system has demonstrated a remarkable sensitivity to mattress vibrations caused by bodily movements, making it proficient in generating complete BCG waveforms capable of discerning breathing and HR patterns, as well as activity. Fig. 1 shows an overview of the proposed RFID-based BCG system. The system comprises two primary components: 1) an active powering board affixed to the bed and 2) a custom-designed passive and flexible sensing board attached to the mattress, positioned opposite and in proximity to the active board. This passive sensing board incorporates two batteryless RFID tags finely tuned to the near-field communication (NFC) frequency of 13.56 MHz.

Both RFID tags within the sensing board harvest energy from the static active board, which remains in a fixed position thanks to a 3-D-printed support structure, as illustrated in Fig. 1. However, the harvested energy serves distinct purposes in each case. One of these tags, referred to as the sensing tag, employs the harvested energy to generate BCG waveforms for the monitoring of the subject's vital signs. The other one, designated as the powering tag, utilizes the harvested energy to power the complete electronic subsystem contained within the sensing tag. The BCG data collected and processed by the sensing tag are wirelessly transmitted to the user's smartphone via an NFC connection. In addition, we have implemented a cloud-based service based on the Message Queue Telemetry Transport (MQTT) messaging protocol, incorporating a broker/client architecture. This facilitates the storage, distribution, and categorization of subject data.

Furthermore, given the placement of the RFID-based sensor on the side of the mattress, it exhibits increased sensitivity to movements near that side, as opposed to those occurring at a greater distance. This setup facilitates the simultaneous monitoring of two subjects by employing two sensing boards positioned on both sides of a queen-size mattress.

II. Related Work

In the field of wireless technology applied to sleep and/or vital signs monitoring, RFID technology has recently emerged as a noteworthy candidate [34], [35], capable of monitoring parameters such as body temperature [36], nocturnal behaviors and activities [37], or respiration [38]. Table I compiles earlier noninvasive systems designed for the monitoring of vital signs in recumbent subjects based on this technology.

As observed in this table, all the preceding systems are contingent upon an external commercial RFID reader and antenna. This RFID reader is responsible for capturing the signals emitted by passive or active tags, which are situated either on the bed or directly on the subject's body, typically in the chest area. Notably, most of these systems capture either the received signal strength indicator (RSSI) or the phase values from the tags to derive vital sign data. Only

TABLE I
COMPARATIVE OF RFID-BASED SENSOR SYSTEMS FOR VITAL SIGNS MONITORING OF INDIVIDUALS LYING ON A BED

Working/sensing principle	Number of sensors	Sensors location	Monitoring capabilities			Two subjects	Generates BCG signal	Transmission method	Ref
			HR	BR	Activity				
Reader captures RSSI values	2 passive tags	User body	No	Yes	No	Yes	No	Reader to PC	[41]
Reader captures RSSI values	8x8 tag matrix	Bed cloth	No	Yes	Yes	No	No	Reader to PC	[42]
Reader captures RSSI values	30x18 tag matrix	Bed sheet	No	Yes	Yes	No	No	Reader to PC	[43]
Reader captures RSSI values	3 passive tags	User body	Yes	Yes	Yes	Yes	No	Reader to PC	[39]
Reader captures RSSI values	2x3 tag matrix	User body	Yes	No	No	Yes	No	Reader to PC	[44]
Reader captures phase info	3 passive tags	User body	No	Yes	No	Yes	No	Reader to PC	[45]
Reader captures phase info	3 passive tags	User body	No	Yes	Yes	Yes	No	Reader to PC	[46]
Tags with accelerometer	3 active tags	Mattress	No	No	Yes	No	No	Reader to PC	[47]
Near-field coherent sensing	1 passive tag	User body	Yes	Yes	Yes	No	Yes	Reader to PC	[40]
Variations in energy harvested by sensing tag	1 passive tag	Mattress side	Yes	Yes	Yes	Yes	Yes	Smartphone app (NFC)	This work

two previous works have been identified that demonstrate the capability to monitor HR, BR, and activity, all the while enabling simultaneous monitoring of two subjects [39], [40]. Nevertheless, in both cases, the sensor needs to be placed on the user body, and the gathered data are transmitted to the user via a commercial RFID reader connected to a PC. It is noteworthy that only one of these systems possesses the ability to generate the BCG signal [40].

In summary, our work presents the following significant contributions.

1) The devised system eliminates the need for an external commercial RFID reader to perform the measurements.
2) Our proposed system can monitor all vital signs of up to two different subjects without necessitating the placement of the sensing tag on the user's body, making it a truly noninvasive system.
3) The collected data can be accessed using any NFC-enabled smartphone via a custom-developed app, removing the requirement for a PC connected to the RFID reader.
4) To the best of the authors' knowledge, our work introduces an innovative RFID-based technique that leverages RFID tags as sensors to generate comprehensive BCG signals.
5) The obtained BCG signals could be used to extract health-related insights, such as detecting heart diseases, respiratory problems, or evaluating sleep quality by identifying sleep stages.

III. SYSTEM ARCHITECTURE AND DESIGN

A. Sensing Mechanism

The developed system primarily comprises two RFID boards, namely, an active board (rigid) and a passive board (flexible). These boards are strategically positioned in proximity, maintaining a fixed separation distance of 3 cm. The flexible passive board, referred to as the "sensing board," is affixed to the mattress side of the bed. The rigid active board, known as the "powering board," is firmly attached to a specially designed 3-D-printed L-shaped support structure. This support structure serves to secure the powering board to the bed, ensuring precise positioning of the entire system at the desired location and separation distance. A schematic representation of the system is illustrated in Fig. 1. The selection of the 3-cm separation distance between the two boards was based on experimental tests. This distance was determined to be optimal, as it enabled the harvesting of sufficient energy from the powering board while achieving good sensitivity in the sensing board.

The generation of the BCG signals using the proposed system is based on the near-field coupling between the powering and sensing boards, which adheres to Faraday's principle of magnetic induction. When the powering board passes a significant alternating current through its coil, it generates a magnetic field in its neighboring area. As the sensing board is placed within this field, a current is induced in the sensing coil antenna. This transfer of energy is harnessed by an RFID/NFC chip connected to the sensing coil, capable of yielding a nonregulated analog output voltage because of the energy harvesting from the magnetic field. This harvested voltage depends on the inductive coupling between the coils, rendering it sensitive to the precise distance and relative positioning of the sensing and powering boards.

The vibrations of the mattress, induced by the bodily movements resulting from the subject's heartbeat and respiration, give rise to minute displacements of the sensing board. These displacements, in turn, lead to slight variations in the alignment between the sensing and powering boards. This subtle misalignment induces changes in the antenna inductive coupling, thereby affecting the harvested energy. Consequently, this results in small fluctuations in the output voltage provided by the RFID/NFC chip. This phenomenon constitutes the central aspect of the proposed sensing mechanism. A continuous recording of this voltage facilitates the generation of a comprehensive BCG signal, enabling real-time monitoring of the subject´s vital signs, including heartbeat, breathing, and activity.

B. Sensing Board Design and Fabrication

The sensing board primarily comprises two battery-less RFID tags printed on a common flexible substrate, both of

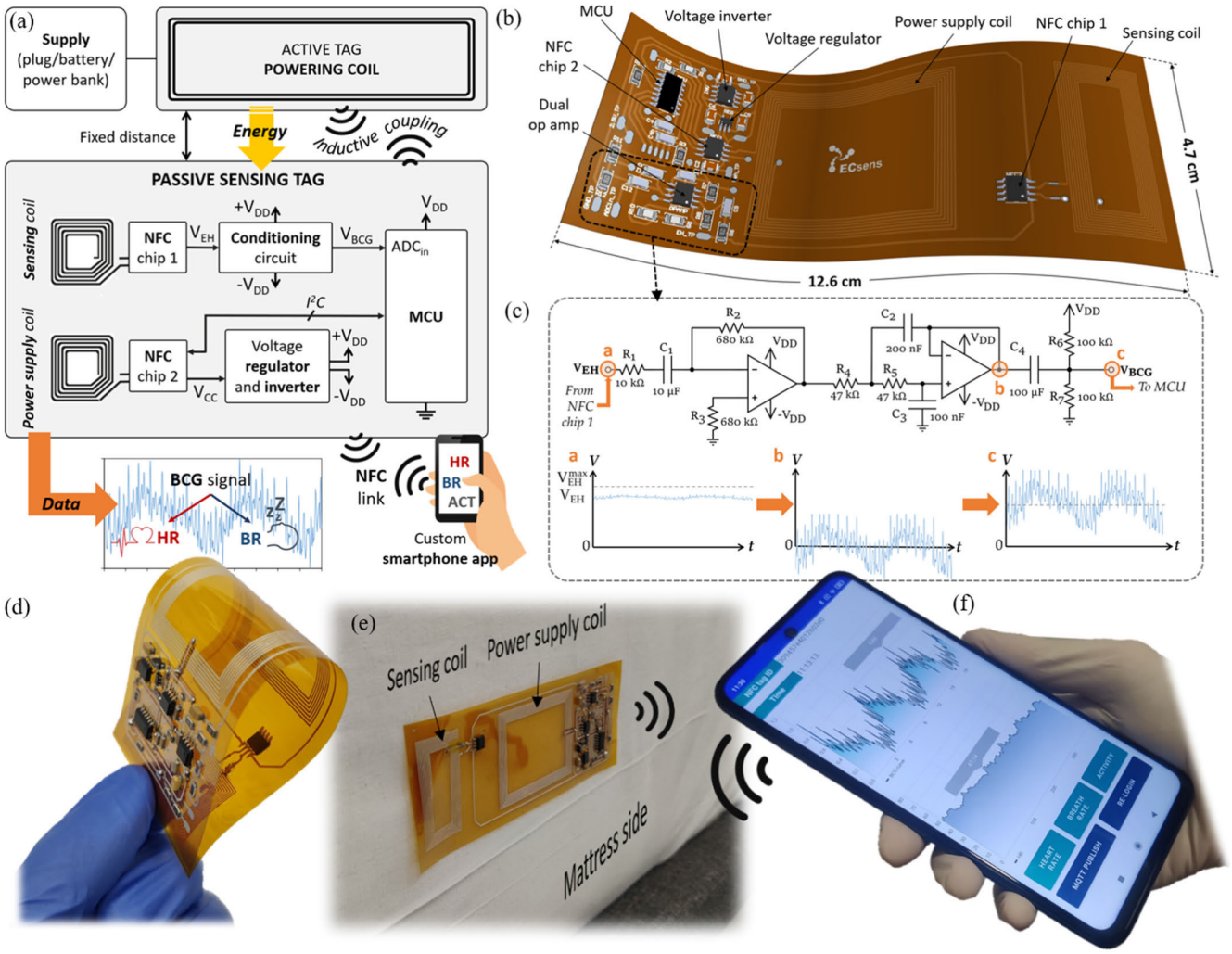

Fig. 2. (a) Block diagram of the BCG system. (b) Layout view of the sensing board. (c) Schematic of the conditioning circuit. (d) and (e) Photographs of the flexible sensing board, also attached to the mattress side. (f) User smartphone running the custom application.

which are based on the ST25DV64KC dynamic NFC/RFID ICs (STMicroelectronics, Geneva, Switzerland). A detailed schematic representation of this board is provided in Fig. 2. One of the key reasons for selecting this chip was its ability to harvest energy from the external RF field generated by the active powering board and provide a nonregulated output voltage. Both RFID tags included in the sensing board leverage the energy harvesting feature for distinct purposes. In one case, variations in the harvested energy available at the analog output pin (V_{EH}) of the first NFC/RFID chip [refer to *NFC chip 1* and the *Sensing coil* in Fig. 2(a) and (b)] are employed to monitor the vital signs of the subject and provide the BCG signal, as previously described.

To achieve this, it is required that the V_{EH} output voltage signal undergoes a conditioning circuit to adapt the voltage harvested by the sensing tag prior to the acquisition by the analog-to-digital (ADC) module of the extreme low-power microcontroller unit (MCU), specifically the PIC16LF1703 model (Microchip Technology Inc., Chandler, AZ, USA). The conditioning circuitry, as depicted in Fig. 2(c), basically consists of three stages. The first stage is a high-pass filter (HPF) with a zero at the origin, aimed at eliminating the dc component of the output signal and amplifying it with a gain of 300. Subsequently, the second stage is a low-pass filter (LPF) with unity gain, designed to remove noise. Both filters were designed using MCP6042 operational amplifiers (Texas Instruments, Dallas, TX, USA). Finally, a dc offset equal to half of the supply voltage is added to the BCG signal through a capacitor in series with a voltage divider. This step results in the V_{BCG} voltage signal, which is acquired and processed by the MCU. This offset voltage is essential to prevent negative voltages at the input of the ADC module.

On the other hand, a second NFC/RFID chip is employed to power the entire sensing board, encompassing the conditioning circuitry and the MCU [refer to *NFC chip 2* and the so-called *Power Supply coil* in Fig. 2(a) and (b). To achieve this, an ultralow-dropout voltage regulator, specifically the model LP2980IM5X-2.5 (Texas Instruments Ltd., Dallas, TX, USA), was connected to the output voltage pin of the second NFC chip (V_{CC}) to obtain a stable output voltage of $V_{DD} = 2.5$ V, derived from the energy harvested from the external RF field. In addition, since the operational amplifiers

require a negative voltage for their rail-to-rail operation, the V_{DD} output voltage provided by the voltage regulator was converted from positive to negative ($-V_{DD}$) using a TL7660 CMOS switched-capacitor voltage converter.

The MCU integrated into the sensing board, responsible for the continuous acquisition of the V_{BCG} voltage, implements a custom-developed algorithm for the extraction of HR, BR, and activity data from the complete BCG signal. Subsequently, the obtained HR, BR, and activity values of the subject are transferred to the EEPROM memory of the NFC chip via the I^2C protocol.

Users can conveniently access these values by simply bringing their smartphone in proximity to the sensing board through a custom-developed application. Furthermore, the smartphone application facilitates the uploading of the acquired data to an MQTT broker, enabling access by MQTT clients, such as a PC or a database. This functionality supports the identification, storage, classification, and distribution of individual subject data, thereby enabling personalized follow-up and individualized control.

Fig. 2(d) and (e) shows the photographs of the fabricated flexible sensing board. This board was manufactured on a flexible Kapton polyimide substrate with a thickness of 125 μm, utilizing a Voltera V-One PCB printer (Voltera Inc., Waterloo, ON, Canada), following a five-step process. First, the circuit layout was printed onto the flexible substrate using a flexible conductive Ag-based ink optimized for the fabrication of flexible circuits (Flex 2, SKU: 1000383, Voltera Inc.). Once the circuit was printed, the ink was cured using the built-in heated platform of the Volterra V-One printer, maintaining a temperature of 200 °C for 35 min. Next, solder paste was dispensed onto the footprints of the components and via pads (T5 Sn42 Bi57.6 Ag0.4, SKU: 1000356, Voltera Inc.). Subsequently, the electronic components and bridges were manually positioned onto their corresponding footprints. Finally, the reflow phase was carried out on the printer's hotplate. The reflow profile encompassed a soak temperature of 180 °C for 45 s, followed by a peak temperature of 220 °C sustained for 30 s.

C. Power Supply and Sensing Coils

The efficient transfer of energy from the active powering board to the passive sensing board depends on how well the loop antennas are tuned to the 13.56-MHz carrier frequency. Therefore, well-designed NFC tag antennas are crucial for optimal performance.

Both sensing and power supply coils within the sensing board were designed based on the chosen RFID/NFC IC, considering that the internal tuning capacitance of this chip is 28.5 pF. The design of the power supply coil was based on the antenna board of the ST25DV64KC discovery kit provided by the manufacturer. This coil has dimensions of 50 × 40 mm with a conductor width (w) of 350 μm, an interspacing (s) of 400 μm between the lines, and a total of $N = 7$ turns.

Conversely, the custom-designed sensing coil features dimensions of 38 × 19 mm, with $N = 10$ turns, an interspacing of 350 μm between the conductor lines, and a width of 200 μm. The initial inductance design for this sensing coil was estimated using the Grover method [48]. The final physical dimensions of the coils were fine-tuned through numerical simulation employing Advanced Design Simulator software (ADS, Keysight Technologies, Santa Clara, CA, USA), a simulation software based on the momentum method. During the simulations, a 1.8-pF capacitance was introduced in parallel with the inductance to account for the probe's parasitic capacitance of the impedance analyzer.

Considering the distinct purposes of each RFID tag in the sensing board, the physical design and placement of the power supply and sensing coils in this board assume paramount significance. On the one hand, the power supply coil must be able to maximize energy harvesting from the RF field generated by the active board, as it serves as the energy source for the entire passive board.

In contrast, the sensing coil should avoid harvesting the maximum attainable energy from the active board. This is a critical requirement, as the subtle variations in the harvested V_{EH} voltage are precisely what enable the system to detect vital signs such as heartbeats and breaths. Therefore, the V_{EH} output voltage of this RFID/NFC chip must never reach its maximum capacity through energy harvesting to prevent signal saturation. If the voltage were to saturate and reach its maximum limit, these crucial variations would cease to exist, rendering the sensing mechanism inoperative.

For this reason, a separation distance of 2.1 cm between the sensing coil and the power supply coil within the passive tag was determined through experimentation. This separation proved to be an effective compromise, allowing for sufficient coupling of the sensing tag without reaching voltage saturation.

Following the establishment of this separation distance, numerical simulations were performed using COMSOL Multiphysics (COMSOL Group, Stockholm, Sweden) to identify the optimal spatial arrangement between the sensing and powering boards. The simulations involved movement along the x-, y-, and z-axes to assess the coupling between the passive sensing board, containing both the power supply and sensing coils, and the active powering board.

In the z-direction, simulations demonstrated that variations in position had minimal impact on the coupling factor, provided that the sensing board remained within the overall dimensions of the active board, with a normalized coupling factor consistently exceeding 0.96. Consequently, the sensing board was positioned in the middle of the active board in the z-direction. In the y-direction, as previously specified, the separation between the boards was experimentally fixed at 3 cm, and the simulation results confirmed a normalized coupling factor of approximately 0.8 at this distance.

The most extensive sweep to determine the optimal location between the sensing and powering boards was conducted along the x-axis direction, as depicted in Fig. 3(a). This figure illustrates the normalized coupling factor as a function of the relative position between the passive sensing coil (in orange), the power supply coil (in blue), and the active powering coil (in green), numerically calculated along the lateral direction (x-axis). The dual objective was to identify a position that maximized the coupling factor of the power supply coil while

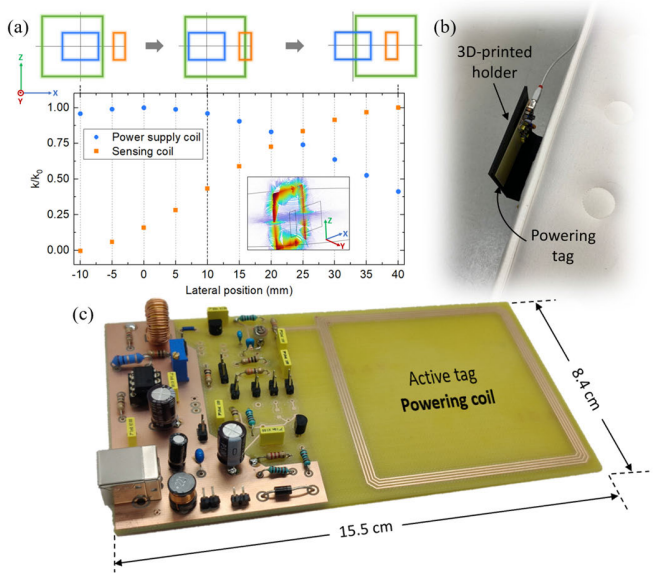

Fig. 3. (a) Normalized coupling factor as a function of the relative position between the sensing and powering boards along the lateral direction (x-axis). (b) Photograph of the powering active board attached to the 3-D-printed L-shaped support. (c) Photograph of the active board based on the Colpitts oscillator circuit.

ensuring that the sensing coil did not reach maximum energy harvesting to prevent output voltage signal saturation. Fig. 3(a) illustrates that the normalized coupling factors of the power supply and sensing coils exhibit contrasting behaviors as the board moves to the right along the x-direction. To meet our specifications, we selected a position that maximized the coupling factor of the power supply coil while maintaining an intermediate level of coupling for the sensing coil. The vertical dashed line in Fig. 3(a) indicates the selected position ($X = 10$ mm), which was subsequently experimentally verified.

In addition, the numerical simulations were also leveraged to determine the direction of maximum variation in the coupling factor between the passive sensing coil and the active powering coil. To achieve this, the derivative of the normalized coupling factor was computed for each case to identify the direction of maximum slope. The outcomes revealed that the coupling factor is notably more responsive to changes in the tags along the y-axis, with a derivative value of 0.022 mm^{-1}. This observation aligns with expectations, as the coupling between the coils experiences a more substantial transformation when the sensing board oscillates back and forth in proximity to the powering board due to the mattress compression and decompression. In situations where a fixed separation along the y-axis is maintained (3 cm in our case), the coupling factor exhibits greater sensitivity to changes in the tags along the z-axis, with a derivative value of 0.018 mm^{-1}, in contrast to the x-axis, where the derivative value is approximately five times lower (0.0038 mm^{-1}). This suggests that micro-movements of the sensing tag along the vertical direction relative to the mattress exert a more pronounced impact on the coupling factor than those along the horizontal direction. In our system, alterations in the coupling factor, and thus the harvested energy, are likely the result of a combination of micro-movements along the y- and z-axes, provoked by changes in the mattress shape.

D. Powering Board Design and Fabrication

To provide wireless power to the sensing board, the active board, as depicted in Fig. 3(c), contains a powering coil oscillating at the frequency of 13.56 MHz.

This board features a common-base Colpitts oscillator circuit [49] that produces a sinusoidal output signal tuned to 13.56 MHz with a power consumption of 650 mW. The circuit comprises a two-terminal LC resonant network connected in parallel with a bipolar transistor amplifier (BJT BC547C, NXP Semiconductors, Eindhoven, The Netherlands). The feedback for the oscillator is provided through a voltage divider composed of two capacitors connected in series across the LC resonant network. For validation, we employed the high-performance HF reader ST25R3911B-DISCO (STMicroelectronics, Geneva, Switzerland), capable of delivering up to 1.4-W output power with a differential antenna. However, our custom-made powering circuit significantly reduces complexity and cost compared to the utilization of this or any other commercial reader.

The printed circuit board (PCB) of this active tag was manufactured using the computer-controlled drilling machine LPKF ProtoMat S100 (LPKF Laser & Electronics SE, Garsen, Germany) on a standard copper-clad 1.5-mm FR4 board. On the other hand, the 3-D-printed L-shaped support, which secures the active powering board and ensures precise system positioning at the required location and separation [see Fig. 3(b)], was designed using the open-source software Wings 3D v2.2.9 and fabricated with a 3-D printer Creality3D model CR-X, employing black PLA filament.

E. Smartphone Application

We have developed a user-friendly application that allows subjects to wirelessly access their monitored data using any NFC-enabled smartphone. When the smartphone is brought near the power supply coil of the sensing board, the application detects and activates the tag. The application features a simple three-button interface that enables users to retrieve data related to HR, breathing, or night-time activity. In each scenario, the smartphone reads and displays two sets of data obtained from the EEPROM memory of the NFC chip, which were previously saved in specific memory locations by the MCU through the I^2C interface [refer to Fig. 2(a)]. As depicted in Fig. 2(f), an upper graph displays the most recent BCG register computed by the extraction algorithm in the MCU, while a lower graph presents the averaged values of HR, BR, or activity (one value per minute) calculated by the algorithm during the entire session.

The smartphone application was created using the integrated development environment (IDE) Android Studio Dolphin 2021.3.1. It was designed and tested on Android 12L (API level 32). However, the application is also compatible with earlier Android versions, with a minimum requirement of Android 5.0 (API level 21). To implement the graphical representation of the BCG signals in the application, we utilized the open-source chart library MPAndroidChart v3.1.0.

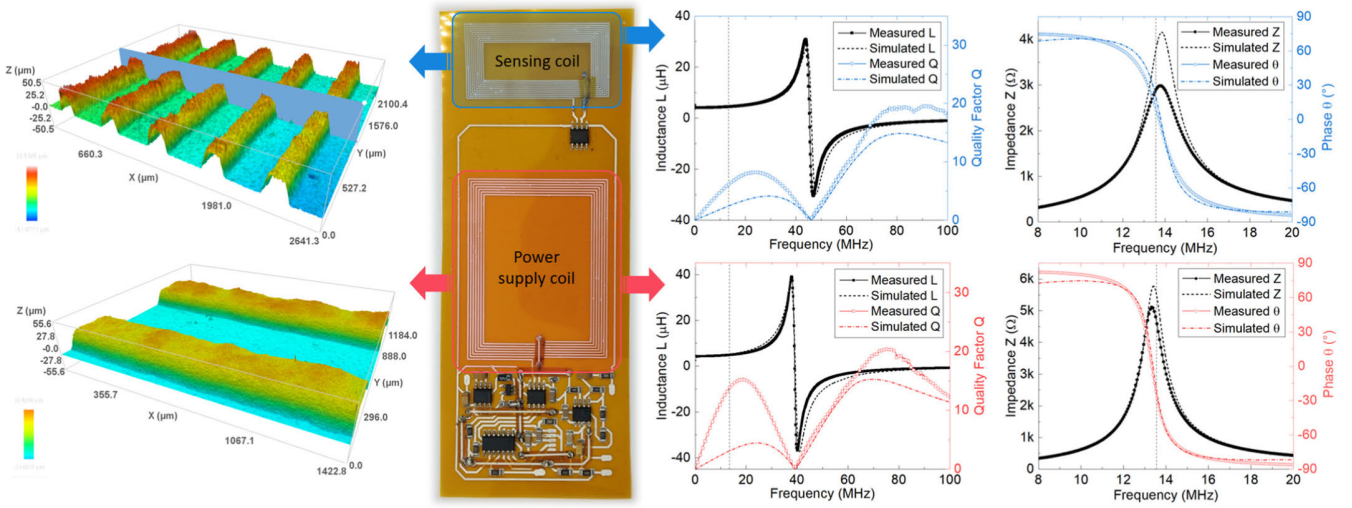

Fig. 4. Simulated and measured frequency responses of the power supply and sensing antennas before and after attaching the RFID/NFC chip (right), along with images of their 3-D profiles measured by the optical profilometer (left).

IV. Results

A. Electromagnetic Performance

To evaluate the electromagnetic performance of the designed RFID tags, numerical simulations and measurements were conducted to analyze the frequency responses of the sensing and power supply coils, both before and after attaching the NFC chip. The results, depicted in Fig. 4 (right), demonstrate a high degree of consistency between the simulated and measured data.

Prior to simulating the frequency response of each antenna coil, surface characterization of the fabricated coils was performed using the 3-D optical profilometer [refer to Fig. 4 (left)]. Both 2-D profiles and 3-D surface images were obtained using an S Neox 3-D Optical Profiler (Sensofar, Barcelona, Spain), accompanied by SensoVIEW 1.6 software. For the sensing coil, an average conductor height of 37.4 $\pm$ 1.1 μm was measured, alongside a conductor width of 181 $\pm$ 15 μm and an interspacing between the lines of 327 $\pm$ 14 μm. In the case of the power supply coil, the measured conductor width was 39.6 $\pm$ 0.7 μm, while the average conductor width was 307 $\pm$ 3 μm, with a spacing of 377 $\pm$ 8 μm. These measured average values were utilized as inputs for the numerical simulations of each coil to closely replicate real-world conditions.

Experimental measurements were performed with a Precision Impedance Analyzer 4294A in combination with an impedance probe kit 4294A1 (Keysight Technologies, Santa Rosa, CA, USA). For the power supply coil, the measured inductance value was 4.903 $\pm$ 0.004 μH at the NFC frequency of 13.56 MHz, closely aligning with the designed value of 4.89 μH, considering that the internal tuning capacitance of the chip is 28.5 pF. After attaching the chip to the coil pads, the power supply antenna exhibited a maximum resonance peak at 13.36 MHz. On the other hand, the sensing coil exhibited an inductance of 4.478 $\pm$ 0.003 μH at 13.56 MHz, with a resonance peak of 13.76 MHz after the NFC chip attachment. These results indicate that both coils are well-suited for communication and energy harvesting through the NFC protocol.

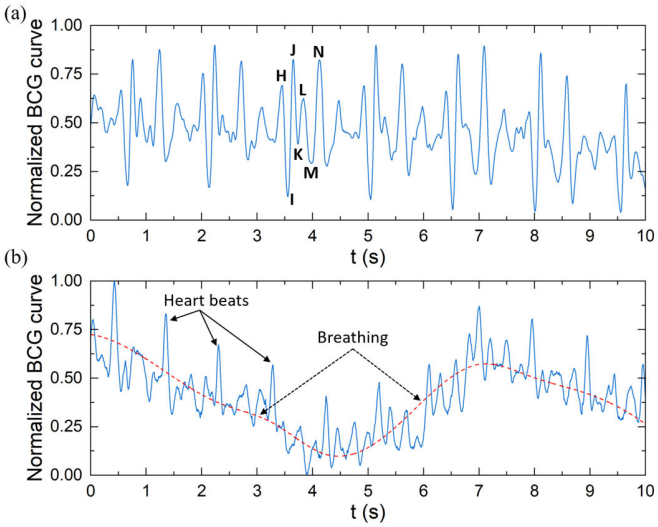

Fig. 5. Examples of two captured BCG curves. (a) Subject holding his breath. (b) Subject deeply breathing.

In terms of power consumption, measurements revealed that the active powering board, positioned at the fixed distance of 3 cm, delivered a power output of 2.29 mW to the passive sensing board. The power consumption of the passive sensing tag was approximately 1.375 mW, equivalent to 550 μA at 2.5 V. This represents roughly 60% of the maximum available power.

B. Ballistocardiogram Signals

The BCG system was initially deployed on an individual mattress measuring 90 $\times$ 180 cm^2 with a height of 21 cm. Fig. 5 provides a detailed illustration of two BCG signals captured using the developed prototype. In Fig. 5(a), during a breath-holding (apnea) episode, the characteristic waves H, I, J, K, L, M, and N [50] are distinctly discernible, with each wave group corresponding to a single heartbeat. Fig. 5(b) illustrates a scenario where the subject was taking deep breaths, resulting in a noticeable rise and fall of the signal baseline synchronized with each inhalation and exhalation.

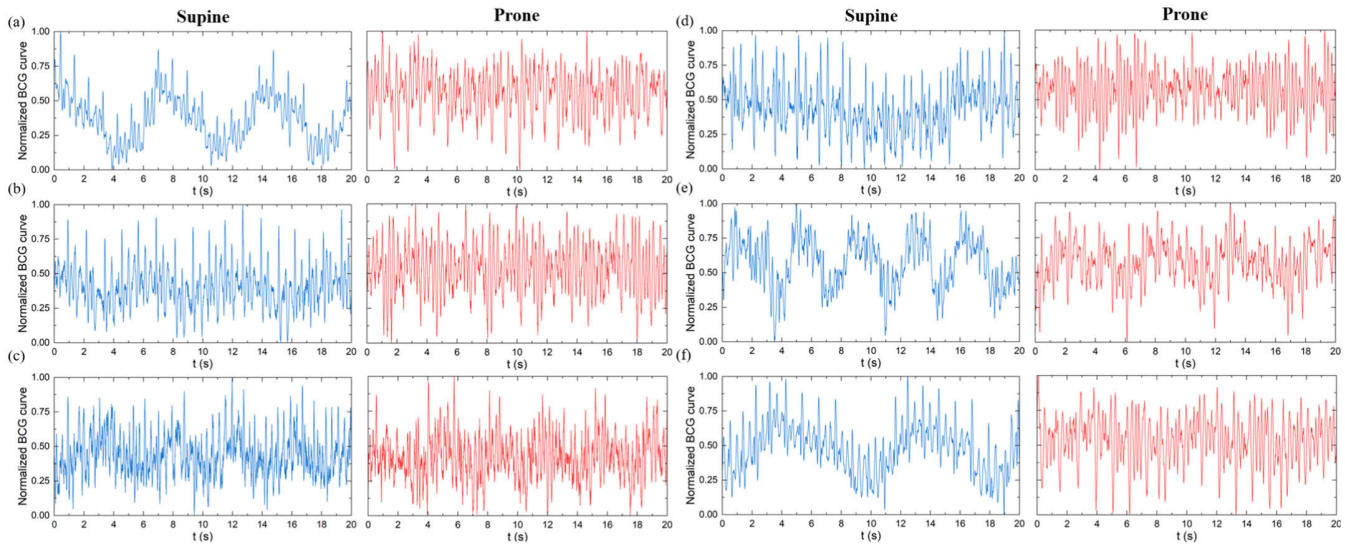

Fig. 6. Acquired BCG curves from six subjetcs (a)–(f) in supine and prone positions. Predicted HR and BR values for them are provided in Table II.

Fig. 6 presents the BCG signals obtained from six different healthy subjects in both supine and prone positions, serving as exemplar signals generated by the proposed system. Descriptive data pertaining to the subjects involved in the recordings are provided in Table III. The figures highlight the distinguishable characteristics of heartbeats, represented by rapid and prominent peaks in the signal, in contrast to the slower and smoother variations attributed to breathing. Notably, in the prone position, the signal baseline oscillation due to the subject's breathing is less pronounced, aligning with expectations in this position.

C. HR and BR Extraction

As elucidated in Section IV-C and discernible from the presented BCG signals, bodily motions induced by heartbeats cause fast fluctuations in the BCG signal, manifesting as peaks. Conversely, breathing engenders a gradual meandering of the signal baseline. Therefore, it becomes feasible to prognosticate the average heart and breath rates by analyzing a sequence of the BCG signal with a specified duration and examining its spectral distribution through the application of the fast Fourier transform (FFT). This analysis assumes regularity in the subject's heartbeats and breathing within the designated time window [51].

The BR can be determined by filtering the sequence samples using an LPF. In this work, a third-order low-pass digital infinite impulse response (IIR) filter with a passband frequency of 0.1 Hz and a stopband frequency of 10 Hz is employed for this purpose. After this filtering process, FFT is applied, and the main non-dc component of the resultant spectrum is designated as the mean BR within this interval. Similarly, the mean HR value is determined following an analogous methodology, albeit replacing the filter with a digital seventh-order IIR HPF characterized by a stopband frequency of 0.1 Hz and a passband frequency of 0.5 Hz.

The described algorithm was applied to the BCG signals shown in Fig. 6, and the obtained results are listed in Table II. The extracted HR values were compared to those obtained through a commercial fingertip pulse oximeter, model JPD-500A (Jumper Medical, Guangdong, China). On the other hand, the BR values were juxtaposed to data directly extracted from the experimental procedure, wherein subjects were prompted to count their breaths—an enumeration further validated through visual inspection of the BCG signals, showing very good agreement. The respective errors for each parameter are incorporated within the table. Overall, the average absolute error for the analyzed sequences was 1.8 beats/min for HR and 0.7 breaths/min for BR. As anticipated from the curves in Fig. 6, the determination of BR in the prone position exhibits greater deviation than in the supine position.

TABLE II
EXTRACTED HR AND BR FOR THE BCG SIGNALS OF FIG. 6

Subject	Supine position		Prone position	
	HR (error) (beats/min)	BR (error) (breaths/min)	HR (error) (beats/min)	BR (error) (breaths/min)
a	63 (2)	9 (0)	63 (2)	6 (2)
b	51 (2)	9 (0)	53 (0)	15 (3)
c	60 (1)	15 (0)	71 (2)	18 (0)
d	45 (3)	6 (1)	48 (3)	8 (2)
e	54 (2)	15 (0)	63 (1)	12 (0)
f	54 (2)	6 (0)	51 (2)	6 (0)

D. Activity Determination

The activity of a lying subject, including leg movement, coughing, or repositioning in bed, among other actions, causes pronounced artifacts in the BCG signal. Such activities result in more intense and rapid motion of the mattress compared to that generated by heartbeats or breathing, both in terms of force and velocity. Consequently, the BCG system reacts to this kind of movement by generating extensive and fast alterations in the signal. Fig. 7 illustrates two instances of BCG signals containing artifacts produced by the subject's activity. In Fig. 7(a), leg movements result in a more pronounced masking effect on the normalized BCG signal compared to

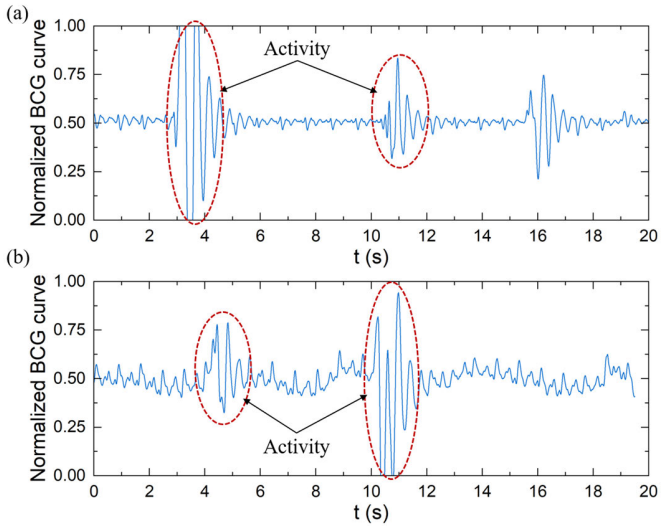

Fig. 7. BCG curves of where activity of the subject is present. (a) Leg movements. (b) Coughing.

the scenario presented in Fig. 7(b), where coughing induces a relatively milder level of activity.

In a previous work, López-Ruiz et al. proposed an algorithm to identify the presence of artifacts caused by the subject's activity during the processing of a given window of the BCG signal. This algorithm relies on calculating the parameter termed the "density of significant samples" for each sequence of samples. This parameter is defined as the normalized number of processed samples with a value higher than the variance measure of the sample set. A high-density value, approaching one, indicates that the sequence is devoid of artifacts induced by the subject's activity, whereas a low-density value, nearing zero, indicates the presence of such artifacts.

In this new proposal for a BCG system, this algorithm was applied to identify artifacts caused by the subject's activity, showing very good performance. In the application of the algorithm, BCG signal samples are initially high-pass filtered to eliminate the dc component and effects of breathing. Subsequently, the samples are squared to maintain a positive sign, and the resulting samples are normalized between 0 and 1. The sequences in Fig. 7 were analyzed using this technique, resulting in a density of significant samples value of 0.15 and 0.22 for the signals shown in Fig. 7(a) and (b), respectively. Given the low values obtained, these sequences are classified as corrupted by the subject's activity, leading to the exclusion of HR and BR extraction during that time interval. Therefore, the algorithm can predict noncardiorespiratory movements of the subject within a given sequence, categorizing them as activity. In such cases, our system lacks the ability to detect heartbeats or breathing during sequences where subject activity is detected. Still, this technique facilitates the precise determination of the moment when the activity occurs, which holds significant importance, particularly in its relevance to sleep stages.

E. Dual-Subject Monitoring

The described prototype was attached to a queen-size mattress measuring 150 × 180 cm^2 with a height of 24 cm.

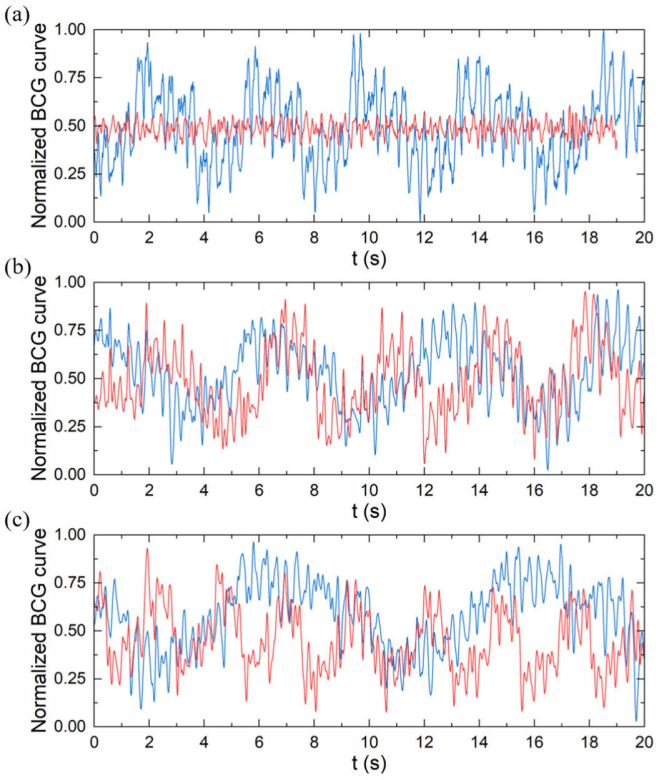

Fig. 8. (a) BCG signals obtained in a queen-size mattress for a subject lying close to the sensor (blue) and on the opposite side of the bed (red). (b) and (c) Simultaneous monitoring of two subjects on a queen-size mattress using independent systems.

To evaluate the system's sensitivity to the subject's distance from the RFID sensor tag, BCG signals were recorded when the subject lays close to the sensor and when positioned on the opposite side of the bed. Fig. 8(a) shows both acquired signals, revealing a substantial reduction in the signal generated when the subject is farther from the sensor. This phenomenon is exploited to enable simultaneous monitoring of two subjects on a queen-size mattress.

In the example depicted in Fig. 8(a), the BR for the blue line (subject close to the sensor) can be precisely determined as 15 breaths/min. However, for the red line, this rate cannot be obtained due to the absence of signal alteration when the subject is lying far from the sensor. The mean HR can be calculated in both cases, resulting in 58 and 60 beats/min for the blue and red lines, respectively. Nevertheless, the signal power, after filtering for HR calculation, is over 12 times higher when the subject is close to the sensor. In terms of spectral density, the power of the component corresponding to the cardiac frequency is more than 35 times higher when the subject is lying close to the sensor. Additional experiments in this direction confirm the system's low sensitivity to mattress motions caused by a subject on the opposite side of the bed.

Consequently, it is expected that a subject lying on the opposite side of a double bed causes minimal cross-interference on the BCG signal generated by a subject resting next to the sensor. These findings lead to the conclusion that two subjects lying on a queen-size bed can be individually monitored using two separate BCG systems as described here and installed on both sides of the mattress.

To demonstrate this, the described setup was implemented on the same queen-size mattress described with two subjects. Fig. 8(b) and (c) illustrates two examples of the BCG signals obtained simultaneously for these two subjects, depicted in blue and red lines. Fig. 8(b) depicts a situation where one subject is relaxed (blue line), and the other is monitored after a brief period of intense exercise. Extracted BR and HR values obtained from the processing of the sequences shown in Fig. 8(b) are 9 breaths/min and 57 beats/min for the relaxed subject, and 15 breaths/min and 93 beats/min for the active subject. Fig. 8(c) shows the signals from two relaxed subjects and one rapidly breathing (red line), while the other one maintains a low and deep breathing (blue line). In this case, both HR and BR are determined as 57 beats/min and 6 breaths/min for the blue line, and 72 beats/min and 24 breaths/min for the red line. This experiment highlights the remarkable capability of our system to simultaneously monitor two subjects on a bed.

V. Discussion

In contrast to conventional BCG systems, which typically require specialized equipment and electrodes, the proposed system seamlessly integrates into a user's existing mattress and wirelessly transmits data to a smartphone, making it convenient and accessible for any user. In addition, wireless operation facilitates bed displacements without compromising functionality. Placing sensors on the side of the mattress makes the system unaffected by bed base characteristics, eliminating the necessity for a rigid board as required by other methodologies. Consequently, the system remains unaffected by bed structure constraints.

However, it is also important to acknowledge certain limitations. First, designing and placing RFID sensing tags is a more intricate process compared to using other conventional sensors in BCG systems, such as film-based sensors or strain gauges. In addition, the precise alignment of the tags is crucial for the proposed algorithm, as signal generation depends on the coupling factor between the tags. Similarly, like other BCG systems, the patient's activity introduces a corrupted signal, making it impossible to extract HR and BR values during active periods.

Despite these limitations, the system's ability to simultaneously monitor two subjects using two sensing boards on a queen-size mattress is a noteworthy feature, potentially serving as a valuable tool for monitoring couples or individuals sharing a bed. This could prove particularly beneficial in scenarios requiring the simultaneous monitoring of multiple individuals. In addition, the cloud service facilitates the storage and distribution of subject data, which could offer healthcare professionals the capability to remotely monitor and analyze the vital signs of patients.

In summary, the proposed BCG system using RFID/NFC technology holds the potential to offer a convenient, accurate, noninvasive, and cost-effective alternative to traditional BCG systems for monitoring the vital signs of individuals lying on a mattress. The use of a limited sample size of six patients in this study serves the purpose of establishing the feasibility and efficacy of our RFID-based sensor system as a proof of concept, rather than conducting a comprehensive clinical trial or product release. This initial phase demonstrates the groundwork and potential for future developments and applications within the field. In this sense, future endeavors will involve conducting statistical studies using various processing algorithms on a larger patient population to extract the parameters of interest. Furthermore, we aim to implement a method for detecting sleep stages based on the extracted parameters and compare the results with polysomnography findings for validation.

TABLE III
Characteristic Data of the Subjects Under Test

Subject	Age (years)	Gender	Weight (kg)
a	42	Male	80
b	54	Male	71
c	19	Female	54
d	45	Male	78
e	37	Female	68
f	34	Male	69

VI. Conclusion

The proposed BCG system, built upon RFID sensing tags, introduces a promising and innovative approach in the field of noninvasive vital sign monitoring. Leveraging RFID/NFC technology, the system has demonstrated remarkable sensitivity to vibrations induced by body movements, enabling the generation of comprehensive BCG signals from which HR, BR, and activity can be extracted. The extraction algorithm, based on the analysis of the spectral distribution of the BCG signal utilizing the FFT, capitalizes on the observation that heartbeats cause rapid variations in the form of peaks, while breathing induces a slow wandering of the signal baseline.

The results obtained from HR and BR extraction exhibit a high level of agreement with those estimated using a commercial fingertip pulse oximeter. Practical trials with six healthy subjects validated the feasibility and efficacy of the system, showing an average absolute error of 1.8 beats/min for HR and 0.6 breaths/min for BR. Beyond HR and BR, the algorithm proficiently filters out artifacts stemming from the subject's activity, such as leg movement, coughing, or rolling over in bed, among others. The BCG system responds to such motions by generating broad and rapid alterations of the signal.

In conclusion, the proposed system presents potential applications across various domains, including hospital settings, home care, and telemedicine. It holds promise for applications such as sleep monitoring, remote patient monitoring, vital signs monitoring in patients with physical limitations, e-health, self-health management, and smart homes, among others.

Appendix

The study was conducted in adherence to the guidelines of the Declaration of Helsinki and received approval from the Ethics Committee in Human Research (CEIH) of the University of Granada (2446/CEIH/2021). Descriptive data for the subjects in the recordings presented in Fig. 6 are provided in Table III. Participants provided written informed consent to partake in the study.

VII. Acknowledgment

The illustration of the subject lying on the bed shown in Fig. 1 was designed by macrovector/Freepik.

References

[1] J. W. Gordon, "Certain molar movements of the human body produced by the circulation of the blood," *J. Anatomy Physiol.*, vol. 11, no. 3, pp. 533–536, Apr. 1877.

[2] Y. Henderson, "The mass-movements of the circulation as shown by a recoil curve," *Amer. J. Physiol.-Legacy Content*, vol. 14, no. 3, pp. 287–298, Sep. 1905.

[3] I. Starr, A. J. Rawson, H. A. Schroeder, and N. R. Joseph, "Studies on the estimation of cardiac ouptut in man, and of abnormalities in cardiac function, from the heart'S recoil and the blood's impacts; the ballistocardiogram," *Amer. J. Physiol.-Legacy Content*, vol. 127, no. 1, pp. 1–28, Jul. 1939.

[4] I. Starr and H. A. Schroeder, "Ballistocardiogram. II. Normal standards, abnormalities commonly found in diseases of the heart and circulation, and their significance," *J. Clin. Invest.*, vol. 19, no. 3, pp. 437–450, May 1940.

[5] W. R. Scarborough, F. W. Davis, B. M. Baker, R. E. Mason, and M. L. Singewald, "A review of ballistocardiography," *Amer. Heart J.*, vol. 44, no. 6, pp. 910–946, Dec. 1952.

[6] L. Giovangrandi, O. T. Inan, R. M. Wiard, M. Etemadi, and G. T. A. Kovacs, "Ballistocardiography—A method worth revisiting," in *Proc. Annu. Int. Conf. IEEE Eng. Med. Biol. Soc.*, Aug. 2011, pp. 4279–4282.

[7] S. Morra et al., "Modification of the mechanical cardiac performance during end-expiratory voluntary apnea recorded with ballistocardiography and seismocardiography," *Physiolog. Meas.*, vol. 40, no. 10, Oct. 2019, Art. no. 105005.

[8] E. Pinheiro, O. Postolache, and P. Girão, "Non-intrusive device for real-time circulatory system assessment with advanced signal processing capabilities," *Meas. Sci. Rev.*, vol. 10, no. 5, pp. 166–175, Jan. 2010.

[9] M. Sidikova et al., "Vital sign monitoring in car seats based on electrocardiography, ballistocardiography and seismocardiography: A review," *Sensors*, vol. 20, no. 19, p. 5699, Oct. 2020.

[10] M. C. Wolf et al., "First feasibility analysis of ballistocardiography on a passenger flight," in *MEDINFO 2019: Health Wellbeing e-Networks for All*. Amsterdam, The Netherlands: IOS Press, 2019, pp. 1648–1649.

[11] O. A. Postolache, P. M. B. S. Girao, J. Mendes, E. C. Pinheiro, and G. Postolache, "Physiological parameters measurement based on wheelchair embedded sensors and advanced signal processing," *IEEE Trans. Instrum. Meas.*, vol. 59, no. 10, pp. 2564–2574, Oct. 2010.

[12] L. Wang, S. Geng, B. Liu, and Y. Jin, "Ballistocardiogram heart rate detection: Improved methodology based on a three-layer filter," *Measurement*, vol. 149, Jan. 2020, Art. no. 106956.

[13] Y. Xu, Z. Yang, G. Li, J. Tian, and Y. Jiang, "A practical application for quantitative brain fatigue evaluation based on machine learning and ballistocardiogram," *Healthcare*, vol. 9, no. 11, p. 1453, Oct. 2021.

[14] J. Liu, F. Miao, L. Yin, Z. Pang, and Y. Li, "A noncontact ballistocardiography-based IoMT system for cardiopulmonary health monitoring of discharged COVID-19 patients," *IEEE Internet Things J.*, vol. 8, no. 21, pp. 15807–15817, Nov. 2021.

[15] M. Drobczyk et al., "Wireless compose-2: A wireless communication network with a ballistocardiography smart-shirt experiment in the ISS columbus module," in *Proc. IEEE Int. Conf. Wireless Space Extreme Environ. (WiSEE)*, Oct. 2021, pp. 103–108.

[16] O. T. Inan, M. Etemadi, R. M. Wiard, L. Giovangrandi, and G. T. A. Kovacs, "Robust ballistocardiogram acquisition for home monitoring," *Physiolog. Meas.*, vol. 30, no. 2, pp. 169–185, Jan. 2009.

[17] Q. Xie et al., "A personalized beat-to-beat heart rate detection system from ballistocardiogram for smart home applications," *IEEE Trans. Biomed. Circuits Syst.*, vol. 13, no. 6, pp. 1593–1602, Dec. 2019.

[18] N. Mora, F. Cocconcelli, G. Matrella, and P. Ciampolini, "Accurate heartbeat detection on ballistocardiogram accelerometric traces," *IEEE Trans. Instrum. Meas.*, vol. 69, no. 11, pp. 9000–9009, Nov. 2020.

[19] R. Song, J. Li, J. Cheng, C. Li, Y. Liu, and X. Chen, "Motion robust imaging ballistocardiography through a two-step canonical correlation analysis," *IEEE Trans. Instrum. Meas.*, vol. 70, pp. 1–10, 2021.

[20] T. Willemen et al., "An evaluation of cardiorespiratory and movement features with respect to sleep-stage classification," *IEEE J. Biomed. Health Informat.*, vol. 18, no. 2, pp. 661–669, Mar. 2014.

[21] G. Garcia-Molina and J. Jiang, "Interbeat interval-based sleep staging: Work in progress toward real-time implementation," *Physiolog. Meas.*, vol. 43, no. 2, Mar. 2022, Art. no. 025004.

[22] J. Tuominen, K. Peltola, T. Saaresranta, and K. Valli, "Sleep parameter assessment accuracy of a consumer home sleep monitoring ballistocardiograph beddit sleep tracker: A validation study," *J. Clin. Sleep Med.*, vol. 15, no. 3, pp. 483–487, Mar. 2019.

[23] J. Alametsä, J. Viik, J. Alakare, A. Värri, and A. Palomäki, "Ballistocardiography in sitting and horizontal positions," *Physiolog. Meas.*, vol. 29, no. 9, pp. 1071–1087, Aug. 2008.

[24] D. U. Uguz, T. B. Tufan, A. Uzun, S. Leonhardt, and C. H. Antink, "Physiological motion artifacts in capacitive ECG: Ballistocardiographic impedance distortions," *IEEE Trans. Instrum. Meas.*, vol. 69, no. 6, pp. 3297–3307, Jun. 2020.

[25] I. Sadek and J. Biswas, "Nonintrusive heart rate measurement using ballistocardiogram signals: A comparative study," *Signal, Image Video Process.*, vol. 13, no. 3, pp. 475–482, Apr. 2019.

[26] K. Watanabe, Y. Kurihara, K. Kobayashi, and K. Suzuki, "Ballistocardiogram (BCG) measurement by a differential pressure sensor," *IEEE Sensors J.*, vol. 21, no. 6, pp. 8583–8592, Mar. 2021.

[27] C. Brüser, A. Kerekes, S. Winter, and S. Leonhardt, "Multi-channel optical sensor-array for measuring ballistocardiograms and respiratory activity in bed," in *Proc. Annu. Int. Conf. IEEE Eng. Med. Biol. Soc.*, Aug. 2012, pp. 5042–5045.

[28] N. López-Ruiz, P. Escobedo, I. Ruiz-García, M. A. Carvajal, A. J. Palma, and A. Martínez-Olmos, "Digital optical ballistocardiographic system for activity, heart rate, and breath rate determination during sleep," *Sensors*, vol. 22, no. 11, p. 4112, May 2022.

[29] I. Sadek, J. Biswas, and B. Abdulrazak, "Ballistocardiogram signal processing: A review," *Health Inf. Sci. Syst.*, vol. 7, no. 1, p. 10, May 2019.

[30] J. C. H. Soto, I. Galdino, E. Caballero, V. Ferreira, D. Muchaluat-Saade, and C. Albuquerque, "A survey on vital signs monitoring based on Wi-Fi CSI data," *Comput. Commun.*, vol. 195, pp. 99–110, Nov. 2022.

[31] V. P. Tran, A. A. Al-Jumaily, and S. M. S. Islam, "Doppler radar-based non-contact health monitoring for obstructive sleep apnea diagnosis: A comprehensive review," *Big Data Cognit. Comput.*, vol. 3, no. 1, p. 3, Jan. 2019.

[32] V. Selvaraju et al., "Continuous monitoring of vital signs using cameras: A systematic review," *Sensors*, vol. 22, no. 11, p. 4097, May 2022.

[33] X. Liu, J. Yin, Y. Liu, S. Zhang, S. Guo, and K. Wang, "Vital signs monitoring with RFID: Opportunities and challenges," *IEEE Netw.*, vol. 33, no. 4, pp. 126–132, Jul. 2019.

[34] P. Escobedo et al., "Smart facemask for wireless CO_2 monitoring," *Nature Commun.*, vol. 13, no. 1, Jan. 2022, Art. no. 1.

[35] S. V. S. T. Jonnalagadda, D. P. Mishra, and S. K. Behera, "Chipless RF identification sensors for vital signs monitoring: A comprehensive review," *IEEE Microw. Mag.*, vol. 24, no. 11, pp. 53–70, Nov. 2023.

[36] F. Naccarata and G. Marrocco, "Integrated wireless RFID temperature sensor for biological aortic valve prostheses," *IEEE J. Radio Freq. Identificat.*, vol. 7, pp. 293–300, 2023.

[37] C. Occhiuzzi, C. Vallese, S. Amendola, S. Manzari, and G. Marrocco, "NIGHT-care: A passive RFID system for remote monitoring and control of overnight living environment," *Proc. Comput. Sci.*, vol. 32, pp. 190–197, Jan. 2014.

[38] S. Zhang, X. Liu, Y. Liu, B. Ding, S. Guo, and J. Wang, "Accurate respiration monitoring for mobile users with commercial RFID devices," *IEEE J. Sel. Areas Commun.*, vol. 39, no. 2, pp. 513–525, Feb. 2021.

[39] R. Zhao, D. Wang, Q. Zhang, H. Chen, and A. Huang, "CRH: A contactless respiration and heartbeat monitoring system with COTS RFID tags," in *Proc. 15th Annu. IEEE Int. Conf. Sens., Commun., Netw. (SECON)*, Hong Kong, Jun. 2018, pp. 1–9.

[40] P. Sharma and E. C. Kan, "Sleep scoring with a UHF RFID tag by near field coherent sensing," in *IEEE MTT-S Int. Microw. Symp. Dig.*, Jun. 2018, pp. 1419–1422.

[41] Z. Hussain, S. Sagar, W. E. Zhang, and Q. Z. Sheng, "A cost-effective and non-invasive system for sleep and vital signs monitoring using passive RFID tags," in *Proc. 16th EAI Int. Conf. Mobile Ubiquitous Syst., Comput., Netw. Services*, Nov. 2019, pp. 153–161.

[42] X. Hu, K. Naya, P. Li, T. Miyazaki, K. Wang, and Y. Sun, "Non-invasive sleeping posture recognition and body movement detection based on RFID," in *Proc. IEEE Int. Conf. Internet Things (iThings) IEEE Green Comput. Commun. (GreenCom) IEEE Cyber, Phys. Social Comput. (CPSCom) IEEE Smart Data (SmartData)*, Jul. 2018, pp. 1817–1820.

[43] J. Liu, X. Chen, S. Chen, X. Liu, Y. Wang, and L. Chen, "TagSheet: Sleeping posture recognition with an unobtrusive passive tag matrix," in *Proc. IEEE INFOCOM Conf. Comput. Commun.*, Apr. 2019, pp. 874–882.

[44] C. Wang, L. Xie, W. Wang, Y. Chen, Y. Bu, and S. Lu, "RF-ECG: Heart rate variability assessment based on COTS RFID tag array," *Proc. ACM Interact., Mobile, Wearable Ubiquitous Technol.*, vol. 2, no. 2, pp. 1–26, Jul. 2018.

[45] C. Yang, X. Wang, and S. Mao, "AutoTag: Recurrent variational autoencoder for unsupervised apnea detection with RFID tags," in *Proc. IEEE Global Commun. Conf. (GLOBECOM)*, Dec. 2018, pp. 1–7.

[46] Y. Wang and Y. Zheng, "TagBreathe: Monitor breathing with commodity RFID systems," *IEEE Trans. Mobile Comput.*, vol. 19, no. 4, pp. 969–981, Apr. 2020.

[47] E. Hoque, R. F. Dickerson, and J. A. Stankovic, "Monitoring body positions and movements during sleep using WISPs," in *Wireless Health 2010*. San Diego, CA, USA: ACM, Oct. 2010, pp. 44–53.

[48] H. Greenhouse, "Design of planar rectangular microelectronic inductors," *IEEE Trans. Parts, Hybrids, Packag.*, vol. PHP-10, no. 2, pp. 101–109, Jun. 1974.

[49] M. A. Carvajal, P. Escobedo, A. Martínez-Olmos, and A. J. Palma, "Readout circuit with improved sensitivity for contactless LC sensing tags," *IEEE Sensors J.*, vol. 20, no. 2, pp. 885–891, Jan. 2020.

[50] J. Gomez-Clapers, A. Serra-Rocamora, R. Casanella, and R. Pallas-Areny, "Towards the standardization of ballistocardiography systems for J-peak timing measurement," *Measurement*, vol. 58, pp. 310–316, Dec. 2014.

[51] K. Watanabe, T. Watanabe, H. Watanabe, H. Ando, T. Ishikawa, and K. Kobayashi, "Noninvasive measurement of heartbeat, respiration, snoring and body movements of a subject in bed via a pneumatic method," *IEEE Trans. Biomed. Eng.*, vol. 52, no. 12, pp. 2100–2107, Dec. 2005.

Pablo Escobedo was born in Jaén, Spain, in 1989. He received the B.Sc. degree in telecommunication engineering, the B.Sc. degree in electronics engineering from the University of Granada, Granada, Spain, in 2012 and 2013, respectively, the M.Sc. degree in computer and network engineering from the University of Granada, in 2014, and the Ph.D. degree in information and communication technologies from the University of Granada in 2018.

He is currently a Post-Doctoral Researcher with the ECSens Group, Department of Electronics and Computer Technology, University of Granada. His research interests include the development of printed sensor systems on flexible substrates, including radio frequency identification (RFID)/near-field communication (NFC) tags with sensing capabilities, for applications in multiple fields such as environmental monitoring, clinical and health analysis/diagnosis, smart packaging of goods and food, and wearable systems for sports activity and biomedical monitoring.

Antonio Pousibet-Garrido was born in La Carolina, Spain, in 1998. He received the B.S. degree in telecommunication engineering and the M.Sc. degree in industrial electronics from the University of Granada, Granada, Spain, in 2021 and 2022, respectively, where he is currently pursuing the Ph.D. degree in information and communication technologies.

His research interests include near-field communication (NFC)-based sensing systems and dosimetry-related studies.

Nuria López-Ruiz was born in Barcelona, Spain, in 1985. She received the B.S. degree in telecommunications engineering, the B.S. degree in electronic engineering, the M.Sc. degree in telecommunications engineering, and the Ph.D. degree in information and communication technologies from the University of Granada, Granada, Spain, in 2008, 2009, 2010, and 2014, respectively.

She is currently an Associate Professor with the University of Granada. Her current research interests include the study of different optical sensors for environmental and biological measurements, the development of paper-based microfluidic platforms, and the design of portable electronic instrumentation and smartphone applications associated with them.

Miguel A. Carvajal was born in Granada, Spain, in 1977. He received the M.Sc. degree in physics, the M.Sc. degree in electronic engineering, and the Ph.D. degree in electronic engineering, with a focus on the development of a dosimeter system based on commercial MOSFETs, from the University of Granada, Granada, in 2000, 2002, and 2007, respectively.

He currently works as a Tenured Professor with the University of Granada. His research interests include the effects of irradiation and post-irradiation in MOSFET transistors, radio frequency identification (RFID) tags with sensor capabilities, gas sensor and electrochemiluminescent sensors, and their applications to handheld instrumentation.

Alberto J. Palma received the B.S. and M.Sc. degrees in physics in 1991 and the Ph.D. degree from the University of Granada, Granada, Spain, in 1995.

He is currently a Full Professor with the Department of Electronics and Computer Technology, University of Granada. Since 1992, he has been working on trapping of carriers in different electronic devices (diodes and MOS transistors) including characterization and simulation of capture cross sections, random telegraph noise, and generation–recombination noise in devices. Since 2000 in the interdisciplinary group ECsens, his current research interests are devoted to the design, development, and fabrication of sensors and portable electronic instrumentation for environmental, biomedical, and food analysis and monitoring. Recently, he has been working on printing sensors on flexible substrates with processing electronics using inkjet and screen-printing technologies.

Antonio Martínez-Olmos was born in Granada, Spain, in 1980. He received the M.Sc. and Ph.D. degrees in electronic engineering from the University of Granada, Granada, in 2003 and 2009, respectively.

He works as an Associate Professor at the University of Granada. His current research interests include the design of sensors for different biological measurements.